L. Damiola, M. Boffadossi, L.M. Pii, A. Rossi, F. Polidoro
Aerothermal Simulation of Gas Turbine Blade Cooling Channel Using Lattice-Boltzmann Method
International Journal of Modern Physics C, Vol. 32, N. 6, 2150080, 2021, p. 1-16
doi:10.1142/S0129183121500807

Aerothermal simulation of gas turbine blade cooling channel using Lattice-Boltzmann method

Luca Damiola*, Maurizio Boffadossi†

Politecnico di Milano, Department of Aerospace Science and Technology, Via La Masa 34 Milano, MI 20156, Italy
**luca.damiola@mail.polimi.it*
†maurizio.boffadossi@polimi.it

Lorenzo M. Pii‡, Alessandro Rossi§

Dassault Systèmes Italia, Viale dell'Innovazione 3 Milano, MI 20126, Italy
‡lorenzomaria.pii@3ds.com
§alessandro.rossi@3ds.com

Francesco Polidoro

Dassault Systèmes SIMULIA Corp., 175 Wyman St Waltham, MA 02451, USA
francesco.polidoro@3ds.com

Received Day Month Year
Revised Day Month Year

Simulations using the Lattice-Boltzmann Method (LBM) are benchmarked to experimental cooling channel studies performed at the Von Karman Institute for Fluid Dynamics. The experimental geometry is representative of a typical rib-turbulated cooling channel for a gas turbine rotor blade. The work aims at describing the flow physics involved, providing a better comprehension of the role of turbulence in augmenting heat transfer. Computations are found to be in agreement with the available experimental data highlighting the accuracy of LBM for aerodynamic and thermal prediction. Results are also compared to Navier-Stokes Large Eddy Simulation (LES). The reduced computational cost compared to LES based methods offers interesting perspectives for future developments.

Keywords: Computational Fluid Dynamics; Lattice-Boltzmann method; Turbulence promoters; Blade cooling; Heat transfer.

PACS Nos.:

1. Introduction

Turbine blades are one of the most critical components in gas turbine engines since they are exposed to significant mechanical and thermal loads, leading to high stresses which can reduce the overall engine life and reliability. Nowadays, typical turbine

inlet temperatures for aeronautical engines are in the order of 1800-1900 K. Despite the considerable progress in material technology, these temperatures are often higher than the material melting point, and they could not be sustained without the assistance of blade cooling technologies. Figure 1 shows the complexity of a typical cooling system employed in modern multipass turbine blades, where several techniques for internal and external cooling are used. The present work focuses on the rib-turbulated internal cooling technique, where the ribs are acting as turbulence promoters. The study provides an aerothermal description of the flow physics that characterizes these particular cooling passages.

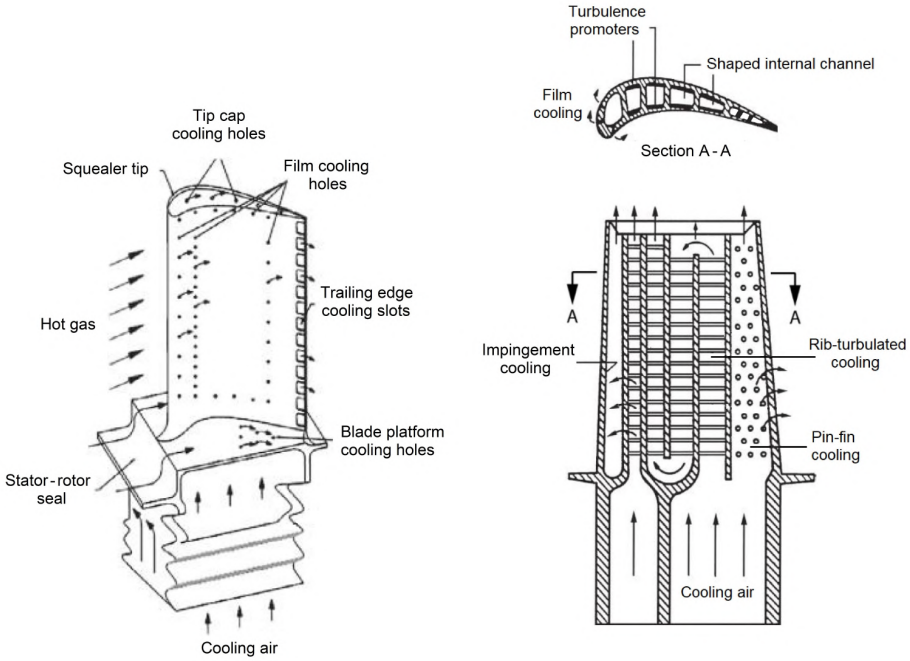

Fig. 1. Typical cooling system of a modern multipass turbine blade.[1]

Previous studies have demonstrated the difficulty of Reynolds Averaged Navier-Stokes (RANS) models to account for complex flow fields involving large flow separation, with results highly dependent on the employed turbulence model. Fransen *et al.*[2] proved the limitations of RANS models for the prediction of separated flows in typical rib-turbulated cooling channels. On the other hand, "scale-resolving" methods such as Large Eddy Simulation (LES), where a portion of the turbulence spectrum is resolved, provide an alternative. In the last few years, the use of LES models for academic research has dramatically increased, but the computational cost remains unaffordable for most industrial applications. The main drawback of LES is related to the requirement in terms of resolution for wall-bounded flows,

which implicate a large number of cells in the wall boundary layers. In this context, the Lattice-Boltzmann solver PowerFLOW which leverages on a Very Large Eddy Simulation (LB-VLES) approach may offer a valid alternative to the traditional numerical methods for Computational Fluid Dynamics, considering a more advanced turbulence modelling compared to RANS and a reduced computational cost compared to LES. Previous work has demonstrated that LB-VLES solvers can reduce the computational cost by 1 to 2 orders of magnitude when compared to LES.[3,4]

In the open literature, Lattice-Boltzmann methods (LBM) have been used for the investigation of separated flows for relatively simple geometries only.[5,6] The present work introduces additional critical features which significantly increase the complexity of the analysis. In particular, the present work investigates the effect of system rotation on the flow field in a typical ribbed channel and, afterwards, presents a detailed heat transfer analysis.

2. Numerical Methodology

Over the past few years, the Lattice-Boltzmann method has rapidly emerged in the field of Computational Fluid Dynamics. This technique is particularly promising because of its ability to account for complex fluids and geometries, and because of its highly parallelizable nature. Differently from the traditional numerical schemes applied in CFD, which characterize the flow motion at a macroscopic level, LBM relies on a mesoscopic description, where particle distribution functions in discrete space and time describe the fluid evolution. This method allows recovering the macroscopic behaviour described by classical Navier-Stokes equations through the Chapman-Enskog asymptotic analysis.[7]

The Lattice-Boltzmann equation, which describes the evolution of the particle distribution function f_i, takes the following form:

$$f_i(\vec{x} + \vec{v}_i \Delta t, t + \Delta t) - f_i(\vec{x}, t) = C_i(\vec{x}, t) \tag{1}$$

The term on the right-hand side of Eq. (1) is known as collision operator and it is often simplified through the Bhatnagar-Gross-Krook (BGK) assumption, namely:

$$C_i(\vec{x}, t) = \frac{1}{\tau}\Big[f_i^{eq}(\vec{x}, t) - f_i(\vec{x}, t)\Big] \tag{2}$$

where τ represents the relaxation time and f_i^{eq} is the equilibrium distribution function. The particle velocity space is discretized into a prescribed number of values, in magnitude and direction. These discrete velocity vectors are such that, in a given time step, a particle is restricted to stream in a limited number of directions. The most adopted scheme is known as the D3Q19 lattice scheme; it was demonstrated that this discretization is sufficient in order to recover the Navier-Stokes equations.[8] The LBM scheme is solved on a cartesian grid composed of

cubic volume elements (voxels), the only exception being the cells which intersect solid boundaries.

After the computation of the distribution function, macroscopic quantities like density, velocity and internal energy are computed by discrete summation, taking the appropriate moments of the distribution function. The remaining quantities are obtained by applying the thermodynamic relations of an ideal gas.

For high Reynolds number flows, the Lattice-Boltzmann equation solver PowerFLOW employs a turbulence modelling based on the solution of a variant of the RNG k-ε model on the unresolved scales, selected via a swirl model.[9] This approach, known as "Lattice-Boltzmann Very Large Eddy Simulation" (LB-VLES), allows limiting the computational cost by computing only the statistically anisotropic eddies outside the Kolmogorov range. In contrast, the unresolved turbulent scales are modelled by replacing the molecular relaxation time scale in the Lattice-Boltzmann equation by an effective turbulent relaxation time scale. The solver also incorporates a turbulent boundary layer model which includes the effect of streamwise pressure gradients.

3. Test Case Description

The numerical analysis performed in the present work reproduces an experimental test case developed for a specific turbomachinery application and recently analyzed at the Von Karman Institute for Fluid Dynamics. The experimental facility, designed by Di Sante *et al.*,[10] is equipped with an on-board Particle Image Velocimetry (PIV) system which allows measurements in the rotating reference frame. Indeed, the system can rotate in the clockwise and counter-clockwise direction at variable rotation speeds. The experimental apparatus allows the measurement of classical mean quantities from uncorrelated time windows, but also of fluctuating quantities resolved in time. These considerations are of great importance in order to accurately validate the unsteady numerical results obtained.

The considered geometry consists of a straight channel with an aspect ratio equal to 0.9, characterized by the presence of eight equally spaced ribs along one wall, as illustrated in Fig. 2. The channel has a rectangular cross-section where the rib blockage ratio is equal to 0.1 and the rib pitch-to-height ratio is 10.

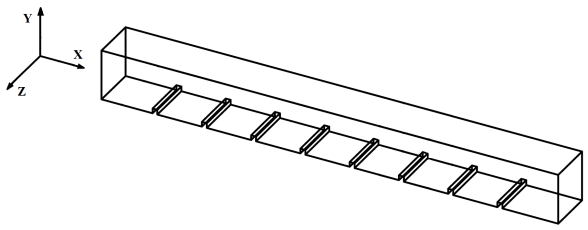

Fig. 2. Sketch of the computational domain.

The Reynolds number, based on the hydraulic diameter and the bulk velocity, is set to 15000. The Prandtl number is equal to 0.72. For this flow condition, PIV measurements are taken in the symmetry plane of the channel. More precisely, the investigated area is limited to the region between the 6^{th} and the 7^{th} obstacle, covering about 1/3 of the channel height.

The numerical results of the present work are benchmarked to the experimental studies performed by Coletti *et al.*[11,12] and Mayo *et al.*[13] In the latter experimental campaign, the experimental facility was slightly modified, introducing three significant changes in the set-up:

- rescaling of the entire test section of a factor equal to 15/8, in order to allow studying flows at higher Reynolds number and rotation number;
- capability to perform Liquid Crystal Thermography (LCT) to investigate the heat transfer performance of the considered geometry at the same conditions as in the PIV experiments;
- variation to the geometry of the channel upstream of the test section, with the introduction of a settling chamber.

In the present work, results are reported in terms of non-dimensional quantities to allow the comparison among the different experimental campaigns.

4. Results

4.1. *Complete cooling channel*

4.1.1. *Numerical details*

The current section investigates the flow field in the same geometry studied experimentally at the Von Karman Institute for Fluid Dynamics. Even though the geometry is relatively simple, the underlying flow physics is complex and very challenging for turbulence modelling.

The boundary conditions for the present numerical analysis represent the closest match with respect to the experimental campaign. In particular, the inflow condition carefully reproduces the velocity profile measured through PIV on the symmetry plane of the channel upstream of the first turbulator; this consists in a turbulent velocity profile characterized by a bulk velocity U_0 = 2.83 m/s and by the same boundary layer height as in the experiments. At the outlet, a uniform ambient static pressure is applied. Finally, no-slip boundary condition is imposed on all solid surfaces. The considered duct is characterized by an hydraulic diameter D_h equal to 79 mm and a rib height h equal to 8 mm. The computational domain is discretized with a Cartesian mesh composed of 25.8 million cubic volume elements (voxels). The use of the variable resolution (VR) technique allows different voxel sizes within the simulation volume, ensuring the correct grid resolution in the domain and, at the same time, reducing the computational effort. The size of the smallest cubic cells in proximity of the wall is equal to 0.2 mm. The simulation time step is set

to 5.86×10^{-6} s, resulting in a Courant-Friedrichs-Lewy (CFL) number equal to unity. The selection of this specific discretization is the result of a thorough grid independence study in which four different meshes composed of a voxel number ranging from 0.6 million to 47.4 million are compared. Since the different grids are obtained by modifying the size of the finest cell, the simulation time step is changed accordingly to guarantee numerical stability. In order to quantify and minimize the numerical errors several indicators are monitored, such as the skin friction coefficient at the bottom wall and the values of the velocity field at specific locations. The selected mesh represents the best trade-off between accuracy of the solution and computational cost, ensuring a complete independence of the solution from the underlying grid.

Results have been obtained by collecting statistics over 0.76 seconds once the flow is statistically established. In this time window, the fluid can go three times from the inlet to the outlet boundary, corresponding to approximately 25 Flow-Through Times (FTT) between two subsequent obstacles.

4.1.2. *Aerodynamic flow field*

A qualitative overview of the present flow field is depicted in Fig. 3, which represents the axial velocity field along the symmetry plane of the channel, non-dimensionalized with the bulk velocity U_0. The main peculiarities are the presence of large recirculation bubbles after the ribs and the strong flow acceleration in the core of the channel due to the rib blockage effect. Moreover, small corner vortices are present just upstream and downstream of the turbulators: the former are caused by the separation of the boundary layer before the rib, whereas the latter are due by the separation induced by an adverse pressure gradient near the bottom wall.

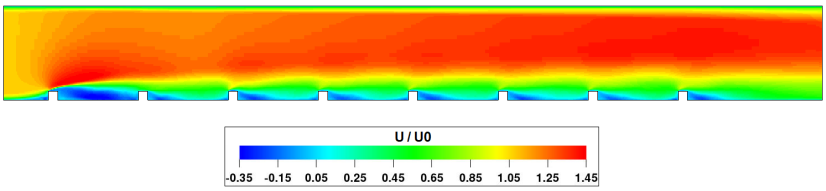

Fig. 3. Non-dimensional streamwise velocity in the symmetry plane of the channel.

The numerical results obtained in this study are compared against the experimental measurements available between the 6^{th} and the 7^{th} obstacle. For the present set-up, that is, the channel in static conditions, the results of two different experimental campaigns are available. Computations are in good agreement with the experimental data, as illustrated in Fig. 4 for the mean (U) and turbulent (U_{rms}) streamwise velocity profiles extracted at several locations in the symmetry plane of the channel. Note that U_{rms} represents the root mean square value of the velocity fluctuations along the streamwise direction.

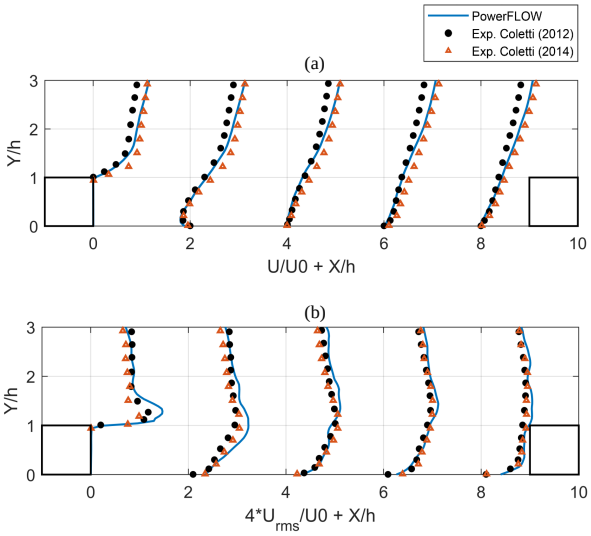

Fig. 4. Mean and turbulent streamwise velocity profiles between the 6^{th} and the 7^{th} turbulator.

4.1.3. *Pressure drop along the channel*

A fundamental aspect concerning the design of a cooling channel is related to the pressure drop induced by the turbulators. An efficient design must be the result of a multi-objective optimization in which the pressure drop is minimized and, at the same time, the turbulence enhancement is maximized to ensure the best heat transfer performance.

In the present work, the total pressure drop as a function of the streamwise coordinate is computed as:

$$\Delta P_{tot}(x) = P_{tot}(x) - P_{tot}^{inlet} \tag{3}$$

where $P_{tot}(x)$ is defined as the total pressure averaged over a transversal slice located at coordinate x and P_{tot}^{inlet} is the average total pressure at the inlet. Figure 5 shows the evolution of the total pressure difference defined in Eq. (3) as a function of the x-coordinate adimensionalized by the rib pitch $P = 80$ mm. Note that, for the sake of clarity, the location of the turbulators has been highlighted using dash-dot lines. It can be observed that each obstacle creates a severe pressure loss with its highest across the first rib. Moreover, the region located between the first and the second rib is characterized by a different pattern compared to the following ones; indeed, as shown in Fig. 3, this area is featured by a much larger recirculation bubble which extends over the entire inter-rib space. The pressure drop over two subsequent turbulators tends to converge to a constant value starting from the 3^{th} rib onwards.

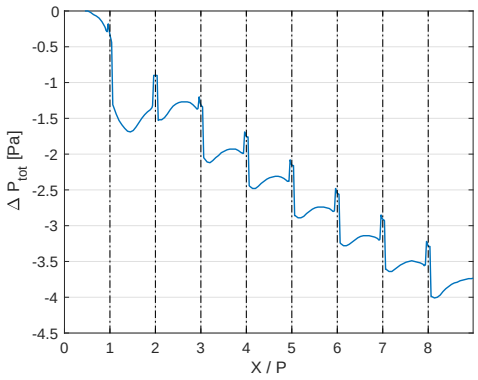

Fig. 5. Total pressure drop along the channel

Based on this graph, the friction factor f of the channel has been calculated according to the following definition:

$$f = \frac{\Delta P_{tot}\, D_h}{2\,\rho\, L\, U_0^2} \tag{4}$$

where L represents the channel length related to the considered pressure drop and D_h defines the hydraulic diameter. The friction factor f has been normalized by the friction factor of a smooth tube f_0, given by the Blasius relation:

$$f_0 = \frac{0.046}{Re^{0.2}} \tag{5}$$

Considering the portion of the channel located between the 4^{th} and the 8^{th} rib, where full convergence is reached, a value $f/f_0 = 2.91$ is obtained. This result is in good agreement with the literature for a similar geometry, characterized by the same rib pitch-to-height ratio $P/h = 10$ and by the same rib blockage ratio $h/D_h = 0.1$.[14]

4.2. *Reduced cooling channel*

4.2.1. *Numerical details*

For the current analysis, the computational domain is reduced to a limited portion of the ribbed channel (see Fig. 6) and the geometry is rescaled by a factor 15/8 as explained in Section 3. The hydraulic diameter D_h is equal to 145 mm and the rib height h is equal to 15 mm. In order to keep the Reynolds number at 15000 the bulk flow velocity is reduced to U_0 = 1.56 m/s. Periodic boundary conditions are applied at inlet and outlet, thus implicitly assuming that the flow field can be considered periodic after the 6^{th} rib. This assumption is proven both experimentally and numerically with an acceptable level of approximation. A no-slip wall boundary condition is applied to all surfaces. The top and lateral walls have an imposed uniform and constant temperature of 293 K, while the bottom

wall has a temperature equal to 314 K. Both these temperature conditions reproduce the experimental setup. The temperature difference causes heat transfer from the floor to the fluid, and from the fluid to the top and lateral walls. Moreover, on the surface of the turbulator, a zero heat flux condition is imposed. The motivation under this simplifying assumption is that in the experimental setup, the rib is built with a low conductivity material and, hence, the heat flux from the turbulator to the fluid can be considered negligible. Finally, in order to match the correct mass flow rate measured in the experimental campaign, a body force aligned with the main flow direction is imposed. It is important to remark that the current analysis takes into account the convective phenomenon, which includes energy transfer due to bulk fluid motion (advection) and random molecular motion (diffusion), whereas wall conduction effects and radiation are not considered. The solver also takes into consideration the coupling between temperature and momentum equations; therefore, the density variation of the fluid due to temperature change is fed back to the momentum equation.

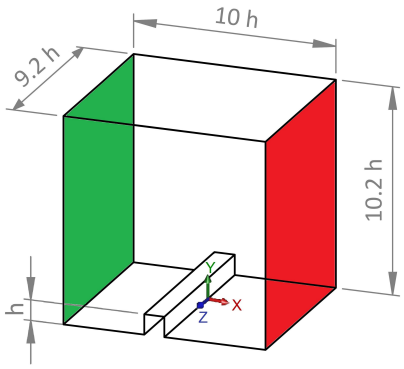

Fig. 6. Sketch of the computational domain: inlet (green) and outlet (red).

The decision to investigate the reduced geometry brought several essential advantages:

- Availability of high fidelity LES results.
- Reduction of the computational effort.
- Possibility to increase mesh resolution without exceeding the available computational power.
- Possibility to simulate a long physical time in order to average data and collect statistics over a large amount of Flow-Through Times (FTT).
- Independence of the solution from small variations in the inflow conditions.

The domain is discretized with a Cartesian mesh composed of 6.1 million cubic elements (voxels). Three different voxel sizes are used in order to ensure high grid resolution in proximity of the walls and in the separated regions, and use less

detail in the central part of the duct. The smallest cubic elements have a dimension of $h/20$, with h being the height of the turbulator. The simulation time step non-dimensionalized using the hydraulic diameter and the bulk velocity is set to 3.8×10^{-4}, resulting in a CFL number equal to unity.

The study is not limited to the static configuration, but also considers the rotating conditions. The idea is to create flow conditions similar to the ones encountered in industrially relevant rotating cooling channels, where the Coriolis and the centrifugal forces actively modify the fluid dynamics. Rotation is prescribed through a methodology often employed in the literature. The approach consists in selecting the rotating frame as the reference frame, and therefore it requires to include the contributions of the Coriolis and the centrifugal forces into the fluid flow equations. The present simulations use a global non-inertial reference frame fixed to the solid geometry, where the angular velocity of the system is prescribed in order to achieve the desired rotation number. The rotation number, defined as $Ro = \Omega D_h / U_0$, is set to ± 0.30 and it expresses the ratio between the Coriolis forces and the inertia forces.

Simulations are performed on 430 cores, and the required computational cost is approximately 1000 total CPU hours for all conditions. More precisely, the time necessary to simulate a single Flow-Through Time is equal to 6.3 CPU hours. Nowadays, these values represent a relatively limited computational effort, which can be easily managed also in an industrial context.

The obtained results are validated against experimental data from Particle Image Velocimetry (PIV) and Liquid Crystal Thermography (LCT), and they are also compared to the numerical simulation performed by Mayo *et al.* using LES.[13–15] Unfortunately, no information concerning the computational effort required by that LES computation is available. In the literature, the only reference providing details on the computational cost required for this kind of internal cooling simulations is given by the publication of Borello *et al.*[16] The authors performed LES computation with a dynamic Smagorinsky model on the same test case analyzed in the present work, but considering a double-length computational domain, consisting in two rib-pitches and periodic boundary conditions imposed at inlet and outlet. The overall number of elements used in the computation is 17.6 million, corresponding to 8.8 million cells for the discretization of a domain length equal to a single rib-pitch. The numerical simulations of Borello *et al.* were performed on the ENEA-Cresco3 and on CINECA-Eurora supercomputers using 64 cores and the authors reported a computational cost which is approximately two orders of magnitude larger compared to the one required by the Lattice-Boltzmann solver PowerFLOW. This difference in computational effort is in accordance with other references in the literature.[3,4]

4.2.2. *Aerodynamic flow field*

The results outlined in the present section have been obtained by averaging data and collecting statistics over a long physical time, corresponding to about 70 FTT after the flow characteristics are statistically established.

Figure 7 shows a very favourable agreement in terms of streamwise velocity among the results obtained with LBM and the data available in the literature. The numerical solution captures accurately the effect of system rotation, which primarily affects the fluid dynamics, actively modifying the shape of the velocity profiles and the size of the recirculation bubble downstream of the rib. The positive rotation reduces the length of the separated region by approximately 10%, whereas the negative rotation leads to a much larger bubble which takes almost the entire inter-rib space. The enlarged area of reverse flow for the negative rotation has a consequence on the rest of the domain as well. Indeed, considering that the Reynolds number is kept constant at 15000 in all three configurations, the broad area of negative axial velocity is balanced by a higher velocity region in the core of the channel.

The different sense of rotation also affects the turbulent levels in the flow. Considering the positive rotation, the turbulent kinetic energy assumes higher values, especially in the region of the turbulators. In this case, in which the ribbed wall represents the pressure side, turbulence is strongly enhanced. As for the negative rotation, the flow is stabilized by the rotation and turbulence is suppressed, since the ribbed wall acts as the suction side.

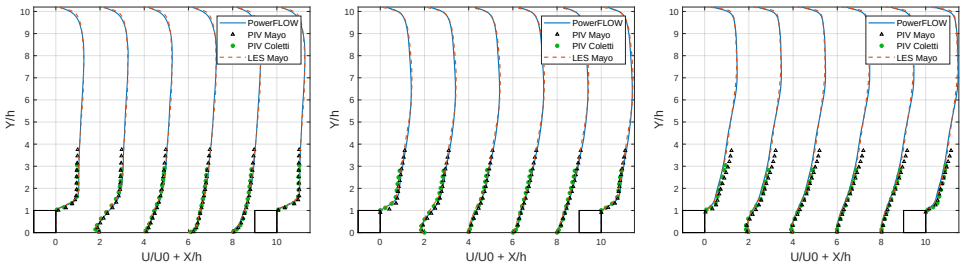

(a) (b) (c)

Fig. 7. Streamwise velocity profiles in the symmetry plane of the channel: positive rotation (a), static (b), negative rotation (c).

4.2.3. *Secondary motions*

A key aspect of the present study is the investigation of secondary motions, which are promoted by the low aspect ratio of the channel. The analysis is conducted considering a section perpendicular to the main flow direction and located downstream of the rib at $X/h = 3.33$. In the static configuration, Fig. 8(a), two large and symmetric counter-rotating vortices occupy a significant portion of the cross-section. Their origin is in the rib-induced secondary flows, which are generated between the rib and the lateral walls and are later advected downstream. As far as the rotating configurations are concerned, the flow field is modified by the Coriolis force, which acts orthogonally to both the main flow direction and the rotation vector. The Coriolis force is proportional to the flow velocity; therefore, a strong effect is expected in the core of the channel. Conversely, a different behaviour characterizes the flow in the vicinity of the lateral walls: in this region, the low axial velocity in the

boundary layer generates a mild Coriolis force which is not sufficient to counteract the transverse pressure gradient locally. The Coriolis force is directed downwards in the case of positive rotation, whereas the negative rotation causes the Coriolis force to act from the bottom wall towards the top wall. In the case of positive rotation, Fig. 8(b), the effect of the Coriolis force strengthens the rib-induced vortices, giving more energy to the secondary motion. For the negative rotation, Fig. 8(c), the Coriolis force overpowers the rib-induced vortices and produces a motion in which the fluid in the proximity of the lateral walls is directed in the negative vertical direction. In addition to the Coriolis-induced secondary flows, the negative rotation also shows the presence of two other counter-rotating cells in the vicinity of the upper wall, which are believed to be originated by the Taylor-Görtler instability.

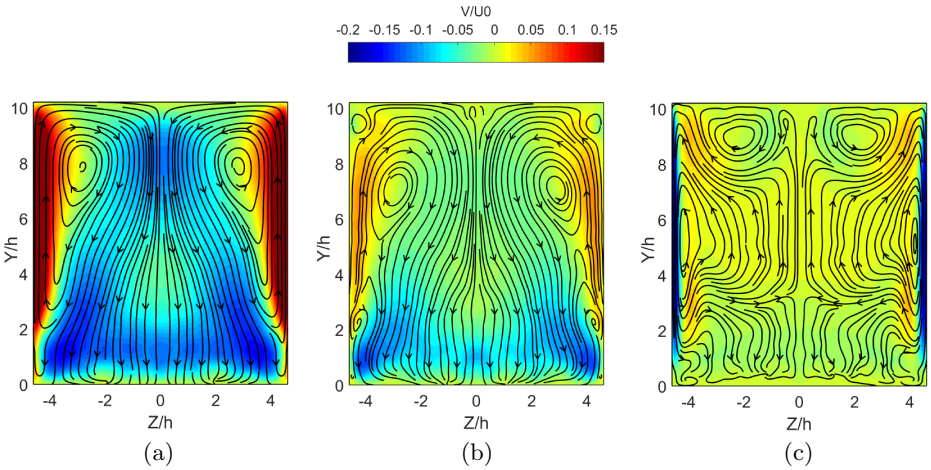

Fig. 8. Streamlines and vertical velocity contours: positive rotation (a), static (b), negative rotation (c)

4.2.4. *Heat transfer analysis*

This part of the work covers a detailed heat transfer analysis which represents a fundamental aspect for turbine blade cooling channels. The parameter commonly employed in order to assess heat transfer is the Nusselt number, which is defined as the ratio between the thermal energy convected to the fluid and the thermal energy conducted within the fluid, namely:

$$Nu = \frac{hD_h}{k} \tag{6}$$

The heat transfer coefficient h is computed as:

$$h = \frac{q_{conv}}{T_w - T_c} \tag{7}$$

where q_{conv} is the convective heat flux at the interface between the fluid and the solid boundary, T_c is the temperature at the centre of the cross-section and T_w is the

temperature of the heated wall. Note that in the definition of the Nusselt number, k represents the thermal conductivity of the fluid computed at film temperature $T_{film} = \frac{1}{2}(T_w + T_c)$.

In the present work the Nusselt number has been normalized by a reference Nusselt number Nu_0 given by the Dittus-Boelter correlation which is valid for a straight smooth circular tube:

$$Nu_0 = 0.023\ Re^{0.8} Pr^{0.4} \tag{8}$$

Therefore, the parameter presented for the evaluation of the heat transfer is called Enhancement Factor and takes the form:

$$EF = \frac{Nu}{Nu_0} \tag{9}$$

In order to have a quantitative representation of the heat transfer evolution in the inter-rib area, the EF is extracted on the centerline of the ribbed wall for the three different rotating conditions, as reported in Fig. 9. The graph shows that the present numerical simulations well capture the heat transfer enhancement/suppression that can be observed in the experimental campaign for the positive/negative rotating configurations, respectively. Moreover, in the case of positive and non-rotating configurations the simulations correctly reproduce the EF reduction starting from $X/h \simeq 4$, which is due to the development of the boundary layer after reattachment. Under negative rotation, the large separation bubble occupies the entire inter-rib space and produces a different EF pattern, which is almost flat in the region $3 < X/h < 8$. Only minor discrepancies are present in comparison to the data available in the literature, partly due to the simplified thermal boundary conditions employed in the CFD simulations.

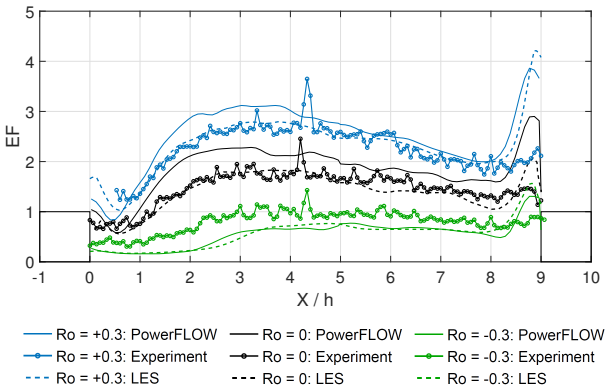

Fig. 9. Comparison of the centerline Enhancement Factor computed on the symmetry line of the ribbed wall.

A more comprehensive understanding of the heat transfer pattern over the entire bottom wall is given by the EF distribution reported in Fig. 10, which shows a different behaviour for the three considered conditions. By taking the static case as the reference configuration, it can be observed that opposite effects are produced depending on the sense of rotation. The counter-clockwise rotation has a destabilizing effect which promotes turbulence enhancement and produces a higher heat exchange between the heated wall and the fluid. On the contrary, under clockwise rotation, the heat transfer capability is significantly reduced due to the turbulence suppression near the ribbed wall and due to the low-momentum caused by the enlarged recirculation bubble.

The rotational effect on the heat transfer performance of the cooling channel is quantitatively evaluated by computing the surface-averaged EF. This value, averaged over the entire inter-rib floor, reveals that the counter-clockwise rotation increases the heat transfer capability by 28%, whereas under clockwise rotation the heat exchanged from the wall to the fluid drastically reduces by 57% compared to the static configuration.

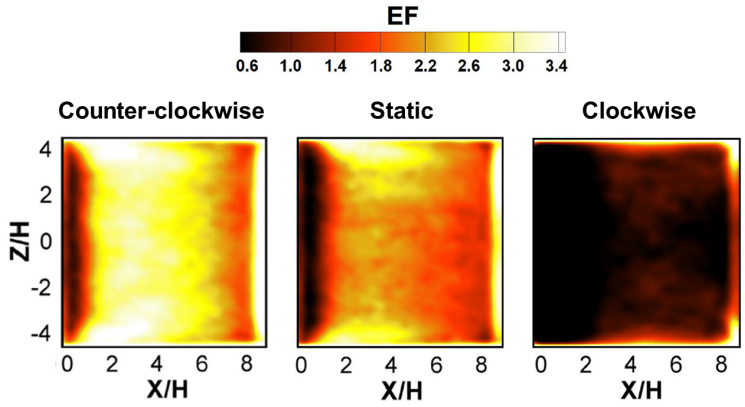

Fig. 10. Enhancement Factor contours on the bottom wall.

5. Conclusions

The present work demonstrated the accuracy of the Lattice-Boltzmann methods for the prediction of aerodynamic and thermal fields in a typical rib-turbulated internal cooling channel. Results showed good accordance with the data available in the literature, denoting the suitability of the solver to account for complex rotating flows.

The numerical simulations allowed to ensure a better understanding of the full three-dimensional flow field, which was only partially investigated in the experimental campaigns. The availability of unsteady measurements over the entire domain revealed turbulence enhancement/suppression depending on the sense of rotation

and allowed a better comprehension of the fundamental role of turbulence in augmenting heat transfer. Finally, the effect of the Coriolis force on the development of secondary motions was highlighted.

The current work has thus presented a detailed aerothermal analysis of the flow physics in a typical rib-turbulated internal cooling channel, providing a similar accuracy compared to more expensive LES based methods. The reduced computational effort offers an exciting perspective for future developments, primarily related to the application of LBM to more realistic geometries.

References

1. J.C. Han, S. Dutta, S. Ekkad, *Gas turbine heat transfer and cooling technology*. CRC press (2012).
2. R. Fransen, N. Gourdain, L.Y. Gicquel, Steady and unsteady modeling for heat transfer predictions of high pressure turbine blade internal cooling. *ASME Turbo Expo 2012: Turbine Technical Conference and Exposition*, 563-572. American Society of Mechanical Engineers Digital Collection (2012).
3. E. Manoha, B. Caruelle, Summary of the LAGOON solutions from the benchmark problems for airframe noise computations-III workshop. In *21st AIAA/CEAS aeroacoustics conference* p. 2846 (2015).
4. A. Maros, B. Bonnal, I. Gonzalez-Martino, J. Kopriva, F. Polidoro, Corner Stall Prediction in a Compressor Linear Cascade Using Very Large Eddy Simulation (VLES) Lattice-Boltzmann Method. In *ASME Turbo Expo 2019: Turbomachinery Technical Conference and Exposition*. American Society of Mechanical Engineers Digital Collection (2019).
5. R.B. Kotapati, R. Shock, H. Chen, Lattice-Boltzmann simulations of flows over backward-facing inclined steps. *International Journal of Modern Physics C*, 25(01), 1340021 (2014).
6. Y. Ma, R. Mohebbi, M.M. Rashidi, Z. Yang, Numerical simulation of flow over a square cylinder with upstream and downstream circular bar using lattice Boltzmann method. *International Journal of Modern Physics C*, 29(04), 1850030 (2018).
7. S. Chapman, T.G. Cowling, D. Burnett, *The mathematical theory of nonuniform gases: an account of the kinetic theory of viscosity, thermal conduction and diffusion in gases*. Cambridge university press (1990).
8. H. Chen, S. Chen, W.H. Matthaeus, Recovery of the Navier-Stokes equations using a lattice-gas Boltzmann method. *Physical Review* A, 45(8), R5339 (1992).
9. C.M. Teixeira, Incorporating turbulence models into the lattice-Boltzmann method. *International Journal of Modern Physics* C, 9(08), 1159-1175 (1998).
10. A. Di Sante, R. Theunissen, R.A. Van den Braembussche, A new facility for time-resolved PIV measurements in rotating channels. *Experiments in Fluids*, 44(2), 179-188 (2008).
11. F. Coletti, T. Maurer, T. Arts, A. Di Sante, Flow field investigation in rotating rib-roughened channel by means of particle image velocimetry. *Experiments in fluids*, 52(4), 1043-1061 (2012).
12. F. Coletti, D.L. Jacono, I. Cresci, T. Arts, Turbulent flow in rib-roughened channel under the effect of Coriolis and rotational buoyancy forces. *Physics of Fluids*, 26(4), 045111 (2014).

13. I. Mayo, G.L. Gori, A. Lahalle, T. Arts, Aerothermal characterization of a rotating ribbed channel at engine representative conditions - Part I: high-resolution PIV measurements. *Journal of Turbomachinery*, 138(10) (2016).
14. I. Mayo, *Flow field and heat transfer in a rotating rib-roughened cooling passage*. PhD Thesis, von Karman Institute for Fluid Dynamics and Institut National Polytechnique de Toulouse (2017).
15. I. Mayo, T. Arts, L.Y. Gicquel, The three-dimensional flow field and heat transfer in a rib-roughened channel at large rotation numbers. *International Journal of Heat and Mass Transfer*, 123, 848-866 (2018).
16. D. Borello, A. Salvagni, K. Hanjalić, Effects of rotation on flow in an asymmetric rib-roughened duct: LES study. *International Journal of Heat and Fluid Flow*, 55, 104-119 (2015).